Inorganic Chemistry

Article

pubs.acs.org/IC

Topochemical Reduction of the Ruddlesden–Popper Phases $Sr_2Fe_{0.5}Ru_{0.5}O_4$ and $Sr_3(Fe_{0.5}Ru_{0.5})_2O_7$

Fabio Denis Romero,[†] Diego Gianolio,[‡] Giannantonio Cibin,[‡] Paul A. Bingham,[§] Jeanne-Clotilde d'Hollander,[§] Susan D. Forder,[§] and Michael A. Hayward*[,†]

[†]Inorganic Chemistry Laboratory, Department of Chemistry, University of Oxford, South Parks Road, Oxford OX1 3QR, United Kingdom

[‡]Diamond Light Source Ltd., Harwell Science and Innovation Campus, Didcot OX11 0DE, United Kingdom

[§]Materials and Engineering Research Institute, Faculty of Arts, Computing, Engineering and Sciences, Sheffield Hallam University, City Campus, Howard Street, Sheffield S1 1WB, United Kingdom

Supporting Information

ABSTRACT: Reaction of the Ruddlesden–Popper phases $Sr_2Fe_{0.5}Ru_{0.5}O_4$ and $Sr_3(Fe_{0.5}Ru_{0.5})_2O_7$ with CaH_2 results in the topochemical deintercalation of oxide ions from these materials and the formation of samples with average compositions of $Sr_2Fe_{0.5}Ru_{0.5}O_{3.35}$ and $Sr_3(Fe_{0.5}Ru_{0.5})_2O_{5.68}$, respectively. Diffraction data reveal that both the $n = 1$ and $n = 2$ samples consist of two-phase mixtures of reduced phases with subtly different oxygen contents. The separation of samples into two phases upon reduction is discussed on the basis of a short-range inhomogeneous distribution of iron and ruthenium in the starting materials. X-ray absorption data and Mössbauer spectra reveal the reduced samples contain an Fe^{3+} and $Ru^{2+/3+}$ oxidation state combination, which is unexpected considering the Fe^{3+}/Fe^{2+} and Ru^{3+}/Ru^{2+} redox potentials, suggesting that the local coordination geometry of the transition metal sites helps to stabilize the Ru^{2+} centers. Fitted Mössbauer spectra of both the $n = 1$ and $n = 2$ samples are consistent with the presence of Fe^{3+} cations in square planar coordination sites. Magnetization data of both materials are consistent with spin glass-like behavior.

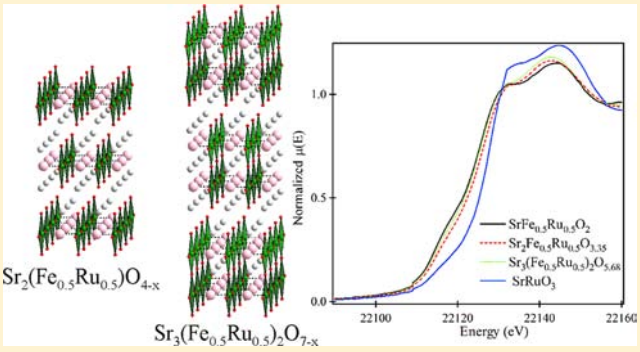

INTRODUCTION

The wide variety of electronic and magnetic behavior exhibited by complex transition metal oxides has motivated an intense and enduring interest in these materials. The diverse array of physical properties exhibited by these systems can be attributed to the presence of electrons in partially occupied metal d orbitals and/or states that are coupled to each other via exchange and other orbital interactions, to yield cooperative, correlated behavior.[1] As a consequence, the electronic structures of complex transition metal oxides depend strongly on the transition metal local coordination geometry and oxidation state, which together define the local transition metal electronic configuration and the connectivity of the extended metal oxide lattice, which defines the nature of the coupling interactions between metal centers. Given the decisive influence these parameters have on determining the physical properties of complex oxides, an effective strategy for discovering new materials that exhibit novel correlated electronic behavior is the preparation of phases that contain transition metal cations in unusual oxidation states and/or coordination geometries embedded within novel metal–oxygen networks.

Conventional high-temperature synthesis routes allow the preparation of a wide range of complex oxide phases. However, although this method is widely employed, it is restricted to preparing only the most thermodynamically stable phases in any composition range, limiting the variety of transition metal oxidation states and coordination geometries that can be realized in the materials formed in this way. In contrast, low-temperature "soft" chemical approaches allow a degree of kinetic control to be applied in formation of reaction products. This allows the preparation of nonequilibrium, metastable phases, extending the range of materials that can be prepared.

Using this approach, binary metal hydrides (NaH, LiH, and CaH_2) have been employed as solid state reducing agents to effect the low-temperature, topochemical reduction of complex, first-row (3d) transition metal oxides.[2−4] This has allowed the preparation of phases with highly unusual transition metal oxidation states and metal coordination geometries, such as square-planar Ni^+, Co^+, Co^{2+}, and Fe^{2+} and even octahedral Mn^+.[2,5−8]

Recently, our attention has turned to complex oxides containing second- and third-row (4d and 5d) transition metals. Initial investigations indicated that under the action of

Received: April 15, 2013
Published: September 16, 2013

strong reducing agents, such as binary metal hydrides, complex 4d and 5d transition metal oxides such as $SrRuO_3$ decompose to the elemental transition metal, via nontopochemical processes, even at low temperatures.[9] However, by incorporating first-row (3d) transition metals, the host lattice can be made sufficiently robust to resist decomposition upon reduction and allow the preparation of topochemically reduced phases. Thus, in contrast to the decomposition of $SrRuO_3$ to SrO and Ru, $SrFe_{0.5}Ru_{0.5}O_3$ can be reduced with CaH_2 to form $SrFe_{0.5}Ru_{0.5}O_2$, a phase in which both the iron and ruthenium cations adopt a square-planar local coordination and the first example of an extended oxide containing Ru^{2+} centers.[9] Magnetic data and density functional theory calculations indicate that the iron centers adopt an $S = 2$, high-spin electronic configuration in common with the all-iron phase $SrFeO_2$,[10] while the ruthenium centers adopt $S = 1$, intermediate-spin configurations, as expected for a 4d transition metal.[9]

In this Article, we describe the reduction chemistry of the $n = 1$ and $n = 2$ $Sr_{n+1}(Fe_{0.5}Ru_{0.5})_nO_{3n+1}$ Ruddlesden−Popper phases to extend the reduction chemistry of complex 4d transition metal oxides.

EXPERIMENTAL SECTION

Synthesis of $Sr_{n+1}(Fe_{0.5}Ru_{0.5})_nO_{3n+1}$ ($n = 1$ or 2). Samples of $Sr_{n+1}(Fe_{0.5}Ru_{0.5})_nO_{3n+1}$ ($n = 1$ or 2) were prepared using a citrate gel method. Suitable quantities of $SrCO_3$ (99.994%), RuO_2 (99.99%, dried at 800 °C for 2 h), and Fe_2O_3 (99.99%) were dissolved in a minimal quantity of a 1:1 mixture of 6 M nitric acid and distilled water. Citric acid and analar ethylene glycol were added, and the solution was heated while being constantly stirred. The gels thus formed were subsequently ground into fine powders, placed in alumina crucibles, and heated in air at a rate of 1 °C/min to 1000 °C to remove the remaining organic components from the samples. The resulting powders were pressed into 13 mm diameter pellets and heated for two periods of 2 days at 1200 °C for the $n = 1$ sample and 1400 °C for the $n = 2$ sample, with regrinding between heating periods, as previously described by Battle et al.[11] The materials produced were observed to be phase-pure by laboratory X-ray powder diffraction, with the following lattice parameters: $a = 3.905(1)$ Å and $c = 12.587(1)$ Å for $Sr_2Fe_{0.5}Ru_{0.5}O_4$, and $a = 3.917(1)$ Å and $c = 20.396(2)$ Å for $Sr_3(Fe_{0.5}Ru_{0.5})_2O_7$ (in good agreement with literature values).[11]

Reduction of $Sr_{n+1}(Fe_{0.5}Ru_{0.5})_nO_{3n+1}$ ($n = 1$ or 2). The reduction of the $Sr_{n+1}(Fe_{0.5}Ru_{0.5})_nO_{3n+1}$ ($n = 1$ or 2) phases was performed using CaH_2 as a solid state reducing agent.[4] To investigate the reactivity of the oxides with CaH_2, small samples (~200 mg) of $Sr_{n+1}(Fe_{0.5}Ru_{0.5})_nO_{3n+1}$ ($n = 1$ or 2) phases were ground together with $2n$ molar equivalents of CaH_2 in an argon-filled glovebox (<1 ppm O_2 and H_2O). The resulting mixtures were then sealed within silica tubes under vacuum and heated at temperatures between 250 and 450 °C for two periods of 2 days with intermediate regrinding.

Due to the hazards associated with the formation of hydrogen gas when performing reduction reactions with CaH_2, large samples suitable for neutron powder diffraction were prepared using a spring-loaded venting apparatus as described previously.[12] Approximately 5 g of the $Sr_{n+1}(Fe_{0.5}Ru_{0.5})_nO_{3n+1}$ ($n = 1$ or 2) phases was ground together with $2n$ molar equivalents of CaH_2 and heated for multiple periods of 2 days at 375 °C with intermediate grinding. After the reaction, samples were washed under nitrogen with 4 × 100 mL aliquots of 0.1 M NH_4Cl in methanol to remove any calcium-containing phases (CaH_2 and CaO) and then washed with a further 4 × 100 mL aliquots of clean methanol before being dried under vacuum.

Synthesis and Reduction of $Sr_{n+1}Ru_nO_{3n+1}$ ($n = 1$ or 2). Samples of Sr_2RuO_4 and $Sr_3Ru_2O_7$ were prepared by a ceramic method. Suitable quantities of $SrCO_3$ and RuO_2 were ground together in an agate pestle and mortar, pressed into pellets, and then heated in air at 1200 °C for 2 days. Samples were then reground and heated for two further periods of 2 days at 1350 °C. As a final step, samples of $Sr_3Ru_2O_7$ were quenched from high temperature into liquid nitrogen to avoid partial decomposition into Sr_2RuO_4 and $SrRuO_3$. X-ray powder diffraction data confirmed the formation of single-phase samples with lattice parameters in good agreement with literature values.[13,14]

Reactions between $Sr_{n+1}Ru_nO_{3n+1}$ ($n = 1$ or 2) phases and $2n$ molar equivalents of CaH_2 were performed in sealed silica tubes. At temperatures below 400 °C, no reaction was observed. At temperatures above 400 °C, reactions of both Sr_2RuO_4 and $Sr_3Ru_2O_7$ resulted in decomposition to form mixtures of SrO, CaO, and elemental ruthenium.

Characterization. X-ray powder diffraction data were collected from samples contained in gastight sample holders using a PANalytical X'Pert diffractometer incorporating an X'celerator position sensitive detector (monochromatic Cu $K\alpha_1$ radiation). Neutron powder diffraction data were collected using the D2B instrument ($\lambda = 1.59$ Å) at the ILL neutron source, from samples contained within vanadium cans sealed under argon with indium washers. Rietveld profile refinements were performed using the GSAS suite of programs.[15] Magnetization data were collected using a Quantum Design MPMS SQUID magnetometer. Thermogravimetric data were collected from powder samples under flowing oxygen using a Netzsch STA 409PC balance.

X-ray absorption experiments were performed at beamline B18 of Diamond Light Source.[16] The measurements were taken using the Pt-coated branch of collimating and focusing mirrors, a Si(111) double-crystal monochromator, and a pair of harmonic rejection mirrors. The size of the beam at the sample position was approximately 600 μm (horizontal) × 700 μm (vertical). XANES data were collected at the Fe K-edge (7112 eV) and at the Ru K-edge (22123 eV) using Si (311) monochromator crystals and Pt-coated mirrors, oriented with a 2.3 mrad grazing incidence angle, for collimation and focusing. A pair of Pd-coated flat mirrors with a 9 mrad incidence angle were used to remove high-energy beam harmonic components for the Fe K-edge measurements.

In both cases, data were collected in transmission mode with ion chambers before and behind the sample filled with appropriate mixtures of inert gases to optimize sensitivity [I_0, 300 mbar of N_2 and 700 mbar of He resulting in an overall efficiency of 10%; I_t, 150 mbar of Ar and 850 mbar of He, with 70% efficiency for Fe K-edge measurements; for Ru-edge measurements I_0 of 250 mbar of Ar and 750 mbar of He and and I_t (I_{ref}) of 350 mbar of Kr and 650 mbar of He]. The spectra were recorded with a step size equivalent to 0.25 eV (1 eV for the Ru K-edge) in continuous scan acquisition mode. Data were normalized using Athena[17] with a linear pre-edge and polynomial postedge background subtracted from the raw $\ln(I_t/I_0)$ data. The samples were prepared in the form of a self-supported pellet, with the thickness optimized to obtain an edge jump close to one.

Room-temperature ^{57}Fe Mössbauer spectra were recorded relative to α-Fe over the velocity range of ±5 mm/s using a constant acceleration spectrometer with a 25 mCi source of ^{57}Co in Rh. Spectra were satisfactorily fit with three broadened Lorentzian paramagnetic doublets using the Recoil analysis software package.

RESULTS

Small-scale test reactions showed no reaction occurred between CaH_2 and either $Sr_2Fe_{0.5}Ru_{0.5}O_4$ or $Sr_3(Fe_{0.5}Ru_{0.5})_2O_7$ at temperatures below 350 °C. Reactions performed at 375 °C yielded new phases that could be indexed on the basis of body-centered orthorhombic unit cells with the following lattice parameters: $a = 3.697(1)$ Å, $b = 3.897(1)$ Å, and $c = 12.877(1)$ Å for the $n = 1$ phase and $a = 3.676(1)$ Å, $b = 3.926(1)$ Å, and $c = 20.798(1)$ Å for the $n = 2$ phase (as determined by X-ray powder diffraction). Reactions performed at temperatures of 430 °C or higher led to sample decomposition.

dx.doi.org/10.1021/ic400930y | Inorg. Chem. 2013, 52, 10920−10928

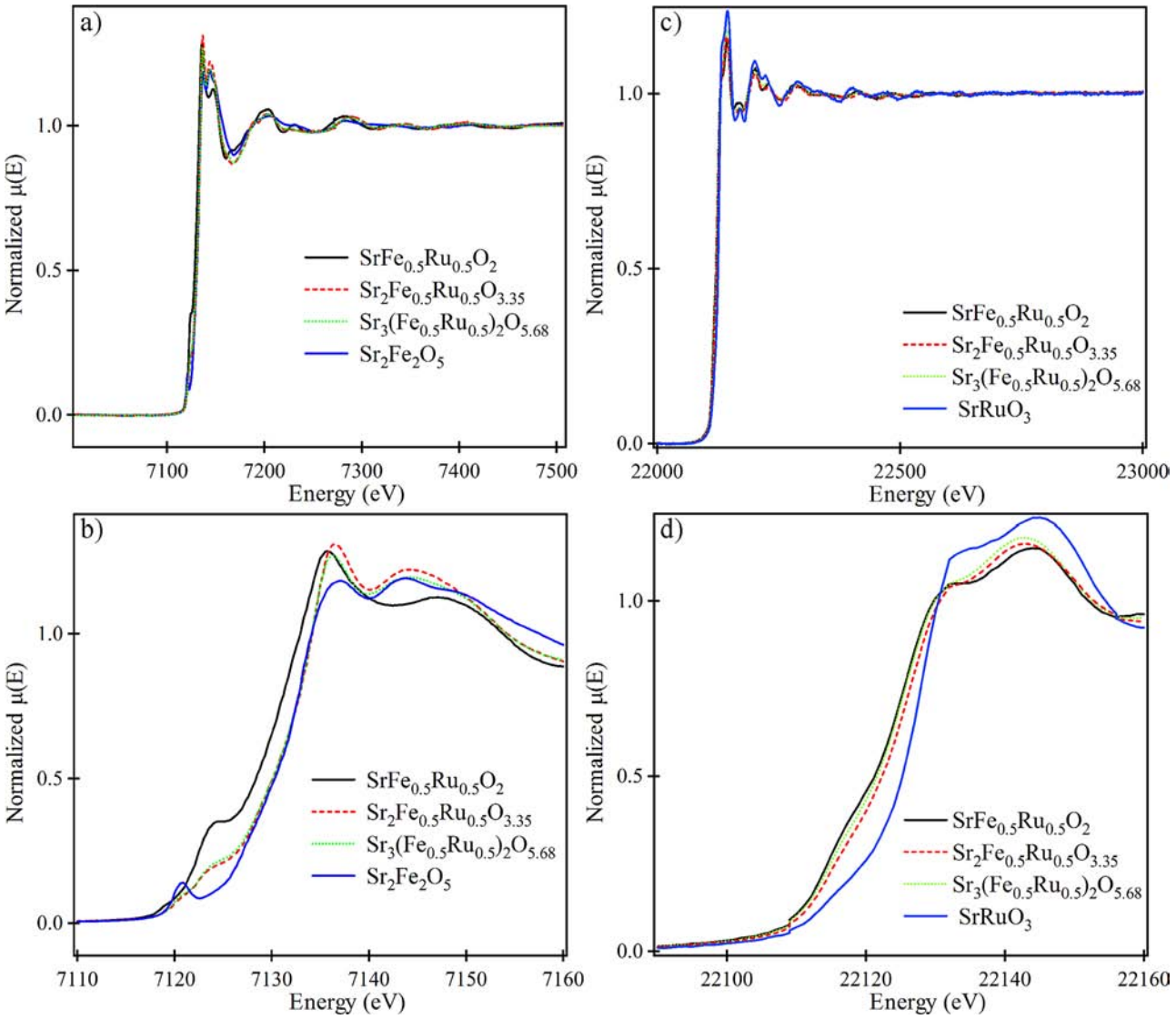

Figure 1. (a and b) Normalized X-ray absorption spectra from the Fe K-edges of $SrFe_{0.5}Ru_{0.5}O_2$, $Sr_2Fe_{0.5}Ru_{0.5}O_{3.35}$, $Sr_3(Fe_{0.5}Ru_{0.5})_2O_{5.68}$, and $Sr_2Fe_2O_5$. (c and d) Normalized X-ray absorption spectra from the Ru K-edges of $SrFe_{0.5}Ru_{0.5}O_2$, $Sr_2Fe_{0.5}Ru_{0.5}O_{3.35}$, $Sr_3(Fe_{0.5}Ru_{0.5})_2O_{5.68}$, and $SrRuO_3$.

Heating the washed products of the reaction between CaH_2 and $Sr_2Fe_{0.5}Ru_{0.5}O_4$ or $Sr_3(Fe_{0.5}Ru_{0.5})_2O_7$ under oxygen led to the reoxidation of these samples back to the oxygen stoichiometric starting materials, as confirmed by X-ray powder diffraction. Thermogravimetric data collected during the reoxidation process were consistent with compositions of $Sr_2Fe_{0.5}Ru_{0.5}O_{3.35(5)}$ and $Sr_3(Fe_{0.5}Ru_{0.5})_2O_{5.68(5)}$ for the two samples (Supporting Information), corresponding to average Fe/Ru oxidation states of +2.70 and +2.68 for the $n = 1$ and $n = 2$ samples, respectively.

X-ray absorption spectra recorded for $Sr_2Fe_{0.5}Ru_{0.5}O_{3.35}$ and $Sr_3(Fe_{0.5}Ru_{0.5})_2O_{5.68}$ show a significant shift to a higher energy of the iron K-edge compared to the equivalent data of the Fe^{2+} phase $SrFe_{0.5}Ru_{0.5}O_2$ (Figure 1a,b).[9] With the exception of the pre-edge features, the Fe absorption edges of $Sr_2Fe_{0.5}Ru_{0.5}O_{3.35}$ and $Sr_3(Fe_{0.5}Ru_{0.5})_2O_{5.68}$ are a good match to the absorption edge of $Sr_2Fe_2O_5$, indicating that iron adopts an Fe^{3+} oxidation state in the reduced Ruddlesden–Popper phases. On the basis of charge neutrality, this would lead to average ruthenium oxidation states in the $n = 1$ and $n = 2$ samples of +2.40 and +2.34, respectively. Support for this assignment can be seen in the Ru K-edge absorption data of $Sr_2Fe_{0.5}Ru_{0.5}O_{3.35}$ and $Sr_3(Fe_{0.5}Ru_{0.5})_2O_{5.68}$ (Figure 1c,d). The ruthenium absorption edges of the $n = 1$ and $n = 2$ samples show the same general shape as the absorption edge of the Ru^{2+} phase $SrFe_{0.5}Ru_{0.5}O_2$ but are shifted to slightly higher energies consistent with average ruthenium oxidation states in the range of +2.3–2.4.

Structural Refinement of $Sr_2Fe_{0.5}Ru_{0.5}O_{3.35}$. Neutron powder diffraction data collected from $Sr_2Fe_{0.5}Ru_{0.5}O_{3.35}$ at 298 K could be readily indexed using a body-centered orthorhombic unit cell. Therefore, a body-centered orthorhombic structural model based on the $n = 1$ Ruddlesden–Popper structure of the $Sr_2Fe_{0.5}Ru_{0.5}O_4$ starting material was prepared in space group *Immm* and refined against these data. When the fractional occupancies of the anion sites were refined, the apical (0, 0, z) site and the equatorial site at (0, $^1/_2$, 0) remained fully occupied, while the occupancy of the equatorial site at ($^1/_2$, 0, 0) declined to ~35%. Close inspection of the fit to the data at this stage revealed a number of peaks were not accurately described (Figures 2a and 3a). Further analysis revealed that h

dx.doi.org/10.1021/ic400930y | *Inorg. Chem.* 2013, 52, 10920–10928

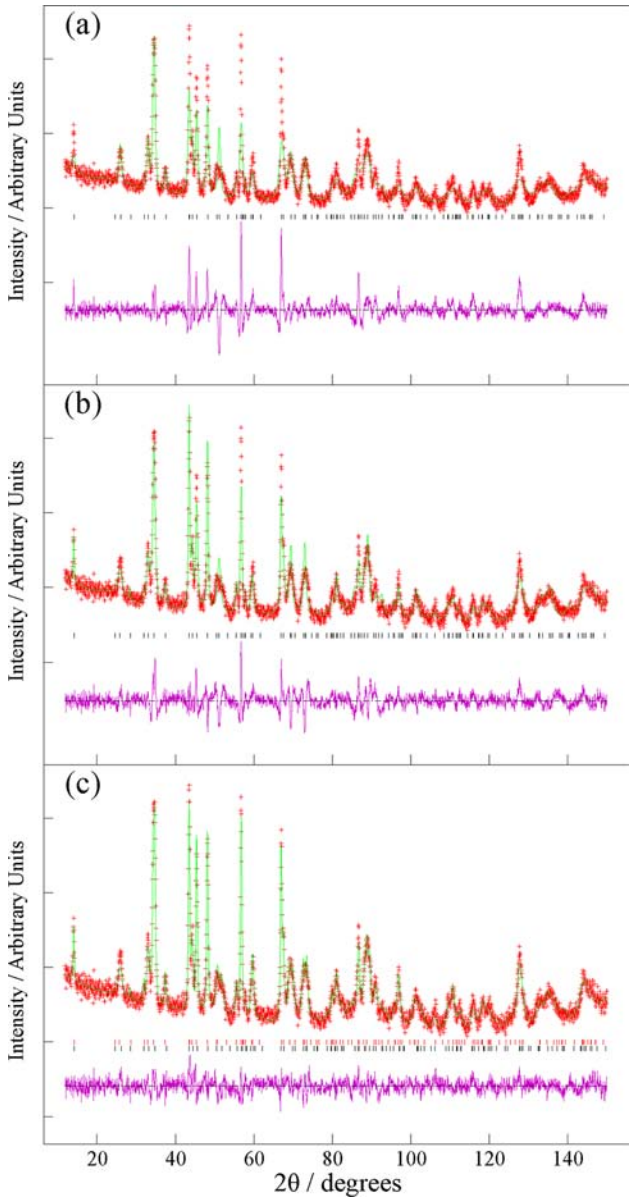

Figure 2. Observed calculated and difference plots from the refinement of (a) a single-phase model, (b) a single-phase model with *hkl*-dependent peak broadening, and (c) a two-phase model against neutron diffraction data collected from $Sr_2Fe_{0.5}Ru_{0.5}O_{3.35}$ at room temperature.

≠ 0 peaks were significantly broader than $h = 0$ peaks, as shown in Table 1. Furthermore, the variation in peak widths could not be readily described using standard anisotropic broadening models (Figures 2b and 3b), suggesting the sample consisted of more than one phase. To fit these unusual peak shapes, a structural model consisting of two orthorhombically distorted $n = 1$ Ruddlesden–Popper phases was used (Figures 2c and 3c). The lattice, structural, and anion occupancy parameters of the two phases were allowed to refine independently, but the thermal displacement parameters of the oxide ions were constrained to be the same within each phase, to improve refinement stability.

This two-phase model converged readily to give a statistical ($\chi^2 = 1.817$) and visual fit to the data (Figure 3c) much improved compared to that of a single-phase model. Observed, calculated, and difference plots for the refinement are shown in

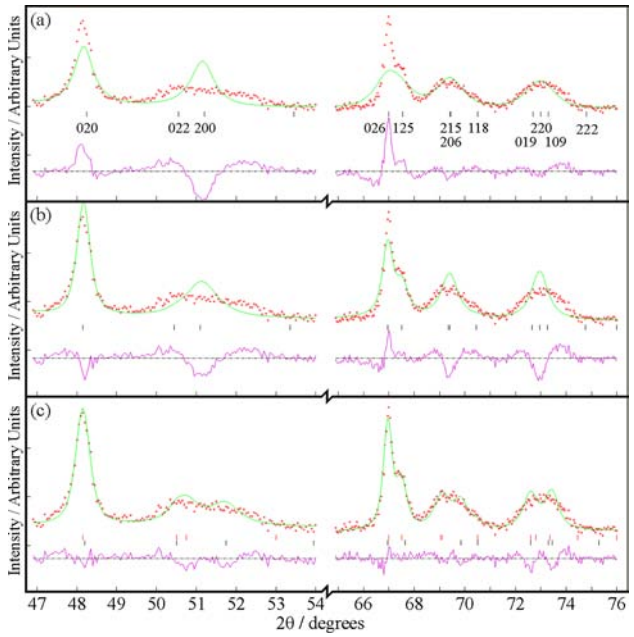

Figure 3. Expanded regions of the observed calculated and difference plots from the refinement of (a) a single-phase model, (b) a single-phase model with *hkl*-dependent peak broadening, and (c) a two-phase model against neutron diffraction data collected from $Sr_2Fe_{0.5}Ru_{0.5}O_{3.35}$ at room temperature.

Table 1. Measured Peak Widths from Neutron Powder Diffraction Data of $Sr_2Fe_{0.5}Ru_{0.5}O_{3.35}$ at 298 K

peak *hkl*	2θ (deg)	full width at half-maximum (deg)
006	43.48	0.595
020	48.14	0.519
200	50.97	2.672
026	66.97	0.533
206	69.86	1.139
220	73.05	1.584

Figure 2c, and full details of the refined structures are listed in Table 2, with selected bond lengths given in the Supporting Information.

The two phases refined against the neutron powder diffraction data, $Sr_2Fe_{0.5}Ru_{0.5}O_{3.25}$ and $Sr_2Fe_{0.5}Ru_{0.5}O_{3.44}$, have very similar *b* and *c* lattice parameters but substantially different *a* lattice parameters (Table 2). In addition, the second phase has a significantly higher anion stoichiometry than the first. The phase-fraction weighted sum of the stoichiometries of the two phases is in good agreement with the average composition obtained from the thermogravimetric data.

Structural Refinement of $Sr_3(Fe_{0.5}Ru_{0.5})_2O_{5.68}$. Neutron powder diffraction data collected from $Sr_3(Fe_{0.5}Ru_{0.5})_2O_{5.68}$ at 298 K could be readily indexed using a body-centered orthorhombic cell (Figure 4). Close inspection of these data revealed the same unusual variation in diffraction peak width with *hkl* index as observed for $Sr_2Fe_{0.5}Ru_{0.5}O_{3.35}$, suggesting the $Sr_3(Fe_{0.5}Ru_{0.5})_2O_{5.68}$ sample also contained more than one phase. Therefore, a structural model based on two orthorhombically distorted $n = 2$ Ruddlesden–Popper phases was refined against the data, in a manner directly analogous to that described above for $Sr_2Fe_{0.5}Ru_{0.5}O_{3.35}$. Once again, a two-phase model was found to fit the data more effectively than a single-phase model ($\chi^2 = 4.071$ for two phases, and $\chi^2 = 7.298$

dx.doi.org/10.1021/ic400930y | *Inorg. Chem.* 2013, 52, 10920–10928

Table 2. Parameters from the Two-Phase Structural Refinement of $Sr_2Fe_{0.5}Ru_{0.5}O_{3.35}$ against Neutron Diffraction Data Collected at 298 K[a]

atom	x	y	z	U_{iso} (Å^2)	fraction
			Phase 1		
Sr(1)	0	0	0.3506(8)	0.004(1)	1
Fe/Ru(1)	0	0	0	0.011(1)	0.5/0.5
O(1)	0	0	0.1580(10)	0.006(2)	1
O(2)	0	1/2	0	0.012(2)	1
O(3)	1/2	0	0	0.012(2)	0.25(1)
			Phase 2		
Sr(1)	0	0	0.3543(7)	0.004(1)	1
Fe/Ru(1)	0	0	0	0.011(1)	0.5/0.5
O(1)	0	0	0.1625(8)	0.004(1)	1
O(2)	0	1/2	0	0.011(3)	1
O(3)	1/2	0	0	0.011(3)	0.44(2)

[a] $Sr_2Fe_{0.5}Ru_{0.5}O_{3.25(1)}$: space group *Immm*, a = 3.6459(7) Å, b = 3.9028(7) Å, and c = 12.898(2) Å. Weight fraction of 47.9(3)%. $Sr_2Fe_{0.5}Ru_{0.5}O_{3.44(2)}$: space group *Immm*, a = 3.7169(8) Å, b = 3.8939(6) Å, and c = 12.856(2) Å. Weight fraction of 52.1(3)%. χ^2 = 1.817. wR_p = 4.78%; R_p = 3.85%.

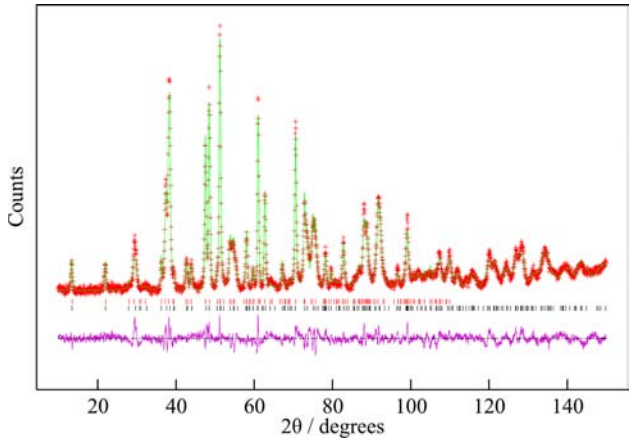

Figure 4. Observed calculated and difference plots from the refinement of a two-phase model against neutron diffraction data collected from $Sr_3(Fe_{0.5}Ru_{0.5})_2O_{5.68}$ at room temperature.

for one; a comparison of single-phase, *hkl*-dependently broadened and two-phase refinements is given in the Supporting Information). Observed calculated and difference plots from the two-phase structural refinement are shown in Figure 4.

Full details of the refined structures are listed in Table 3, and selected bond lengths are given in the Supporting Information. In common with the two-phase model of $Sr_2Fe_{0.5}Ru_{0.5}O_{3.35}$ described above, the two phases refined against the neutron diffraction data collected from $Sr_3(Fe_{0.5}Ru_{0.5})_2O_{5.68}$ have very similar b and c lattice parameters but substantially different a lattice parameters (Table 3) and significantly different oxygen stoichiometries.

Mössbauer Spectra. Mössbauer spectra of $Sr_2Fe_{0.5}Ru_{0.5}O_{3.35}$ and $Sr_3(Fe_{0.5}Ru_{0.5})_2O_{5.68}$ are shown in Figures 5 and 6. Both spectra can be fit by three overlapping doublets: a pair of doublets corresponding to Fe^{3+} centers (sites 1 and 2) that account for ~98% of the area of both spectra and a further weak doublet (site 3) that corresponds to a low concentration of Fe^{4+} centers. Despite the small contribution of the Fe^{4+} sites to the spectra of both samples, the presence of this site is

Table 3. Parameters from the Two-Phase Structural Refinement of $Sr_3(Fe_{0.5}Ru_{0.5})_2O_{5.68}$ against Neutron Diffraction Data Collected at 298 K[a]

atom	x	y	z	U_{iso} (Å^2)	occupancy
			Phase 1		
Sr(1)	0	0	1/2	0.004(1)	1
Sr(2)	0	0	0.3163(3)	0.004(1)	1
Fe/Ru(1)	0	0	0.0968(3)	0.002(1)	0.5/0.5
O(1)	0	0	0.1948(3)	0.022(4)	1
O(2)	0	0	0	0.022(4)	1
O(3)	0	1/2	0.0972(4)	0.018(3)	1
O(4)	1/2	0	0.0972(4)	0.018(3)	0.25(1)
			Phase 2		
Sr(1)	0	0	1/2	0.012(2)	1
Sr(2)	0	0	0.3129(4)	0.012(2)	1
Fe/Ru(1)	0	0	0.0991(6)	0.011(3)	0.5/0.5
O(1)	0	0	0.1961(6)	0.081(1)	1
O(2)	0	0	0	0.081(1)	1
O(3)	0	1/2	0.0898(6)	0.101(10)	1
O(4)	1/2	0	0.0898(6)	0.101(10)	0.43(3)

[a] $Sr_3(Fe_{0.5}Ru_{0.5})_2O_{5.50(2)}$: space group *Immm*, a = 3.6553(5) Å, b = 3.9300(3) Å, and c = 20.815(2) Å. Weight fraction of 49.8(15)%. $Sr_3(Fe_{0.5}Ru_{0.5})_2O_{5.86(6)}$: space group *Immm*, a = 3.7164(5) Å, b = 3.9208(4) Å, and c = 20.740(2) Å. Weight fraction of 50.2(15)%. χ^2 = 4.01. wR_p = 5.61%; R_p = 4.22%.

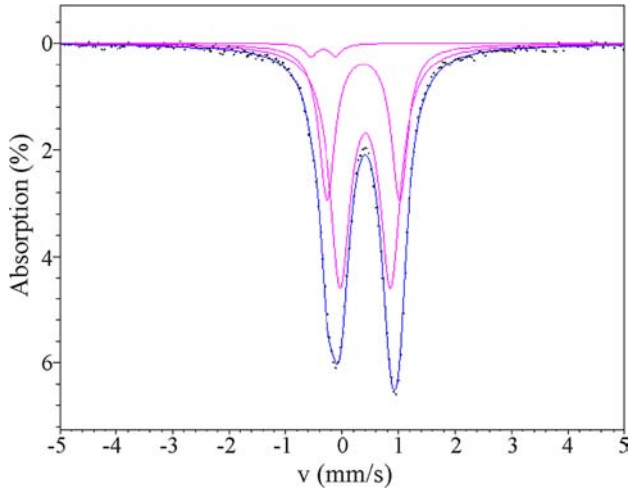

Figure 5. Fitted ^{57}Fe Mössbauer spectrum of $Sr_2Fe_{0.5}Ru_{0.5}O_{3.35}$ at room temperature.

supported by a visually observed shoulder in the data, and the inclusion of this doublet significantly improves the fit to both spectra, as demonstrated by comparison of the χ^2 values associated with the two-doublet and three-doublet fits given in the Supporting Information. Details of the three-doublet fits to both spectra are listed in Table 4.

Magnetic Characterization. Magnetization data collected as a function of temperature from $Sr_2Fe_{0.5}Ru_{0.5}O_{3.35}$ in an applied field of 100 Oe reveal a divergence between the zero-field cooled and field cooled data at T ~ 260 K and a local maximum in the zero-field cooled data at T ~ 20 K (Figure 7). Analogous magnetization data collected as a function of temperature from $Sr_3(Fe_{0.5}Ru_{0.5})_2O_{5.68}$ show a divergence at T ~ 20 K (Figure 7). Neither data set could be fit to the Currie–Weiss law over any significant temperature range.

dx.doi.org/10.1021/ic400930y | *Inorg. Chem.* 2013, 52, 10920–10928

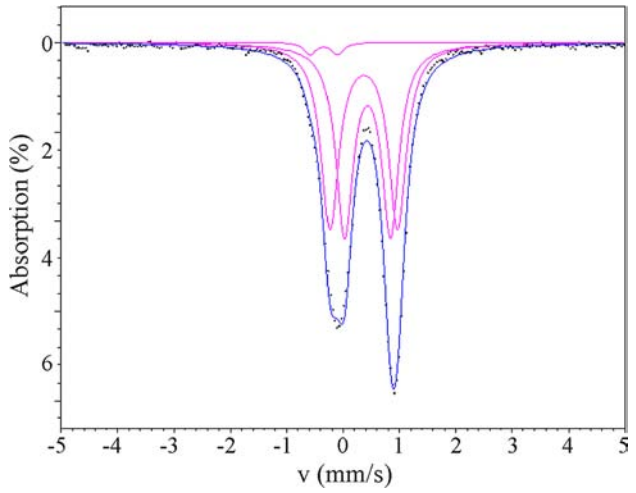

Figure 6. Fitted ^{57}Fe Mössbauer spectrum of $Sr_3(Fe_{0.5}Ru_{0.5})_2O_{5.68}$ at room temperature.

Table 4. Parameters Extracted from Fitting Fe Mössbauer Spectra of $Sr_2Fe_{0.5}Ru_{0.5}O_{3.35}$ and $Sr_3(Fe_{0.5}Ru_{0.5})_2O_{5.68}$

	$Sr_2Fe_{0.5}Ru_{0.5}O_{3.35}$			$Sr_3(Fe_{0.5}Ru_{0.5})_2O_{5.68}$		
	site 1	site 2	site 3	site 1	site 2	site 3
center shift ± 0.02 (mm/s)	0.41	0.38	−0.34	0.43	0.37	−0.34
quadrupole splitting ± 0.02 (mm/s)	0.89	1.29	0.44	0.82	1.20	0.48
line width ± 0.02 (mm/s)	0.22	0.17	0.12[a]	0.18	0.19	0.12[a]
area fraction ± 1 (%)	64.1	34.0	1.9	48.9	49.0	2.1
reduced χ^2	1.17			3.44		

[a]Line width constrained to this value to ensure appropriate fitting.

Magnetization-field data collected from both the n = 1 and n = 2 samples at 5 K exhibit hysteresis and are displaced from the origin, suggesting spin glass-like behavior (Figure 7). No evidence of long-range magnetic order was observed in neutron powder diffraction data collected at 5 K from either sample.

Two-Phase Reduction Behavior. The separation of both $Sr_2Fe_{0.5}Ru_{0.5}O_4$ and $Sr_3(Fe_{0.5}Ru_{0.5})_2O_7$ into two distinct phases upon reduction is rather unusual. To investigate this further, a series of test reactions were performed by heating mixtures with a 1:2 molar ratio of $Sr_2Fe_{0.5}Ru_{0.5}O_4$:CaH_2 in sealed silica ampules at 375 °C for multiple periods of 2 days, until the X-ray diffraction patterns of the products no longer changed between heating periods. These test reactions utilized $Sr_2Fe_{0.5}Ru_{0.5}O_4$ samples prepared in separate batches as described above. It should be noted that all the batches of $Sr_2Fe_{0.5}Ru_{0.5}O_4$ were identical as determined by diffraction.

X-ray powder diffraction data revealed that all the test reactions produced products that were two-phase mixtures of topochemically reduced $Sr_2Fe_{0.5}Ru_{0.5}O_{4-x}$ phases. As shown in Table 5, the lattice parameters of the reduced product phases are very similar to those refined against the neutron diffraction data from the large sample, indicating that the same two phases are produced regardless of the batch of $Sr_2Fe_{0.5}Ru_{0.5}O_4$ used. However, the relative fractions of the two phases in the reduced products, while constant if the same batch of $Sr_2Fe_{0.5}Ru_{0.5}O_4$ was used, varied between batches of $Sr_2Fe_{0.5}Ru_{0.5}O_4$, indicating that some subtle feature of the starting material was influencing the phase separation upon reduction.

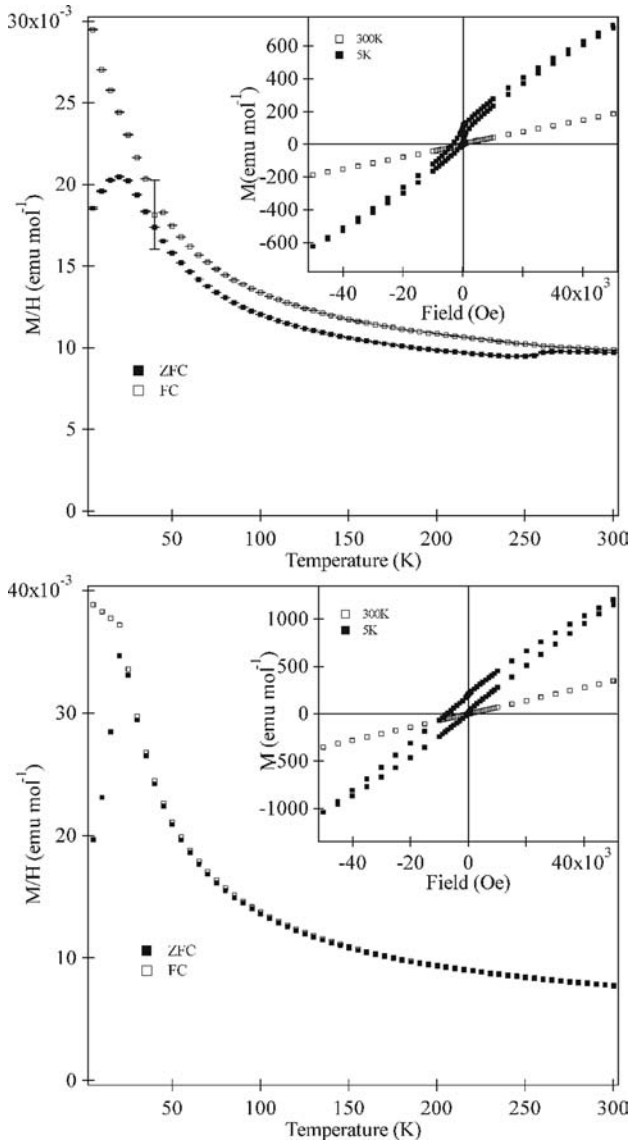

Figure 7. Zero-field cooled and field cooled magnetization data from $Sr_2Fe_{0.5}Ru_{0.5}O_{3.35}$ (top) and $Sr_3(Fe_{0.5}Ru_{0.5})_2O_{5.68}$ (bottom). Insets show magnetization isotherms collected at 300 and 5 K.

DISCUSSION

Reaction of the n = 1 and n = 2 Ruddlesden−Popper phases Sr_2RuO_4 and $Sr_3Ru_2O_7$ with CaH_2 leads to the decomposition of the extended oxide phases, resulting in mixtures of SrO and elemental ruthenium that are produced in nontopochemical reactions analogous to those seen previously for $SrRuO_3$.[9] However, substitution of 50% of the ruthenium with iron stabilizes the extended metal oxide lattice; thus, reaction of $Sr_2Fe_{0.5}Ru_{0.5}O_4$ and $Sr_3(Fe_{0.5}Ru_{0.5})_2O_7$ with CaH_2 leads to the reductive, topochemical, deintercalation of oxide ions from the $(Fe_{0.5}Ru_{0.5})O_2$ equatorial planes of these phases, to yield materials with average compositions of $Sr_2Fe_{0.5}Ru_{0.5}O_{3.35}$ and $Sr_3(Fe_{0.5}Ru_{0.5})_2O_{5.68}$, respectively. Powder diffraction data show that the reduced products formed from both the n = 1 and n = 2 $Sr_{n+1}(Fe_{0.5}Ru_{0.5})_nO_{3n+1}$ starting materials consist of two phases, which retain the cation lattice of the respective parent phase but have differing oxygen stoichiometries. Thus, the n = 1 product is a 47.9:52.1 mixture of $Sr_2Fe_{0.5}Ru_{0.5}O_{3.25}$ and

dx.doi.org/10.1021/ic400930y | Inorg. Chem. 2013, 52, 10920−10928

Table 5. Lattice Parameters and Phase Fractions Extracted from the Two-Phase Samples Prepared by the Reaction of $Sr_2Fe_{0.5}Ru_{0.5}O_4$ and CaH_2 at 375 °C

	phase 1				phase 2		
batch	a (Å)	b (Å)	c (Å)	phase ratio	a (Å)	b (Å)	c (Å)
neutron	3.645(1)	3.902(1)	12.898(2)	48:52	3.716(1)	3.893(1)	12.856(2)
X-ray 1	3.666(2)	3.889(3)	12.897(3)	42:58	3.723(4)	3.901(3)	12.865(6)
X-ray 2	3.633(2)	3.893(2)	12.905(3)	51:49	3.731(2)	3.906(2)	12.856(6)

$Sr_2Fe_{0.5}Ru_{0.5}O_{3.44}$, and the n = 2 product is a 49.8:50.2 mixture of $Sr_3(Fe_{0.5}Ru_{0.5})O_{5.50}$ and $Sr_3(Fe_{0.5}Ru_{0.5})O_{5.86}$.

Reactivity of $Sr_{n+1}(Fe_{0.5}Ru_{0.5})_nO_{3n+1}$ Phases. The relatively low level of reduction achieved (average transition metal oxidation states of $M^{+2.70}$ and $M^{+2.68}$ for n = 1 and n = 2, respectively) and the separation into two phases observed when the $Sr_{n+1}(Fe_{0.5}Ru_{0.5})_nO_{3n+1}$ (n = 1 or 2) phases react with CaH_2 are quite unlike those observed from the related all-iron phases $SrFeO_3$ and $Sr_3Fe_2O_7$ and the iron/ruthenium perovskite phase $SrFe_{0.5}Ru_{0.5}O_3$, all three of which undergo reduction reactions with CaH_2 to form single-phase products with average transition metal oxidation states of M^{2+}.[9,10,18] Given that both the n = 1 and n = 2 $Sr_{n+1}(Fe_{0.5}Ru_{0.5})_nO_{3n+1}$ phases form very similar products upon reduction [an approximate 1:1 mixture of $Sr_{n+1}(Fe_{0.5}Ru_{0.5})_nO_{2.25n+1}$ and $Sr_{n+1}(Fe_{0.5}Ru_{0.5})_nO_{2.43n+1}$ phases], it seems likely there is a common explanation for the unusual reactivity of these two materials.

Reviewing the reaction conditions required to reduce the all-iron phases, we observe that $SrFeO_{3-\delta}$ is reduced to $SrFeO_2$ at 280 °C,[10] while a temperature of 350 °C is required to reduce $Sr_3Fe_2O_{6+x}$ to $Sr_3Fe_2O_5$,[18] suggesting that the n = 2 Ruddlesden–Popper phase has an energetic barrier to oxide ion migration higher than that of the perovskite phase. Considering that the iron–ruthenium phase $SrFe_{0.5}Ru_{0.5}O_3$ is reduced to $SrFe_{0.5}Ru_{0.5}O_2$ at 400 °C, we would expect the reduction of iron–ruthenium Ruddlesden–Popper phases to materials containing Fe^{2+}/Ru^{2+} centers to require reaction temperatures considerably in excess of 400 °C.[9] However, as noted above, reduction reactions performed at temperatures above 430 °C result in the decomposition of n = 1 and n = 2 $Sr_{n+1}(Fe_{0.5}Ru_{0.5})_nO_{3n+1}$ phases. Thus, we can see that the limited level of reduction observed upon reaction between $Sr_{n+1}(Fe_{0.5}Ru_{0.5})_nO_{3n+1}$ (n = 1 or 2) phases and CaH_2 arises because the anion mobility in these materials is not significantly greater than that of the cation lattice, so that at the temperatures required to reduce these phases to Fe^{2+}/Ru^{2+} materials, the cation lattice is sufficiently mobile to prevent topochemical reactions from occurring and thus nontopochemical, thermodynamic reaction products result (e.g., SrO + Fe + Ru).

The separation of both $Sr_2Fe_{0.5}Ru_{0.5}O_4$ and $Sr_3(Fe_{0.5}Ru_{0.5})_2O_7$ into two separate phases upon reduction is unexpected, although not unprecedented. A number of complex oxide phases have previously been observed to undergo phase separation on reduction, and this behavior has previously been attributed to a number of different factors. For example, the n = 1 Ruddlesden–Popper phase $LaSrCoO_4$ forms two phases on reaction with dilute hydrogen gas, $LaSrCoO_{3.43}$, and $LaSrCoO_{3.57}$, due to incomplete reaction (compared with the analogous reaction with NaH) and inhomogeneous reaction conditions through the sample during reduction.[19] In contrast, the two-phase behavior observed on reduction of the pyrochlore phase $Y_2Ti_2O_7$ can be explained on the basis of a compositional "phase gap" driven by the electronic structure of the material, so that materials with average compositions in the range $Y_2Ti_2O_{7-x}$ ($0.65 < x < 5.90$) are two phase mixtures of $Y_2Ti_2O_{6.5}$ and $Y_2Ti_2O_{5.90}$.[20] However, neither of these situations provides a convincing explanation for the two-phase behavior observed in the Fe/Ru phases because, as noted above, the molar ratio of the two product phases formed upon reduction of $Sr_{n+1}(Fe_{0.5}Ru_{0.5})_nO_{3n+1}$ materials does not evolve over time, once established. This is not the case for the $LaSrCoO_{4-x}$ or $Y_2Ti_2O_{7-x}$ system; in both cases, the reduction reactions are still proceeding and are expected to produce single-phase samples given sufficient time. This leads to the conclusion that the observed two-phase $Sr_{n+1}(Fe_{0.5}Ru_{0.5})_nO_{3n+1}$ reduction products do not arise from incomplete reaction or electronic phase separation but occur because different portions of the sample react with CaH_2 to different extents, despite being subject to the same chemical and thermal conditions. This suggests that the phase separation observed upon reduction arises because the n = 1 and n = 2 starting materials are inhomogeneous in some way; that is to say, they already consist of a mixture of phases, and the reduction process just brings this inhomogeneity to light. This view is reinforced by the observation that the ratio of $Sr_{n+1}(Fe_{0.5}Ru_{0.5})_nO_{3n+1}$ reduced product phases is reproducible within each "batch" of starting material but that different batches yield different ratios of reduced products (Table 5).

Close inspection of diffraction data collected from the n = 1 and n = 2 starting materials shows no evidence of compositional inhomogenity. In addition, the structural models refined against data collected from the reduced materials (Tables 2 and 3) show no indication of uneven iron/ruthenium segregation between the product phases for either the n = 1 or n = 2 system, indicating that on the length scale probed by diffraction, samples have a homogeneous iron/ruthenium distribution. The Mössbauer spectra of both $Sr_2Fe_{0.5}Ru_{0.5}O_{3.35}$ and $Sr_3(Fe_{0.5}Ru_{0.5})_2O_{5.68}$, however, suggest that over short length scales this is not the case, as detailed below.

Previous studies of $Sr_{n+1}(Fe_{0.5}Ru_{0.5})_nO_{3n+1}$ phases indicate that the transition metals adopt an Fe^{3+}/Ru^{5+} oxidation state combination, as demonstrated by Mössbauer and magnetic data.[11,21,22] The observation of small but clear Fe^{4+} signals in the Mössbauer spectra of $Sr_{n+1}(Fe_{0.5}Ru_{0.5})_nO_{3n+1-x}$ phases after reduction is therefore unexpected. The most plausible explanation for observing Fe^{4+} in the product phases after reduction is that Fe^{4+} centers were present in the starting material prior to reduction and have not been reduced by CaH_2. The presence of Fe^{4+} centers in the starting materials is consistent with the presence of very small iron-rich and ruthenium-rich regions in the $Sr_{n+1}(Fe_{0.5}Ru_{0.5})_nO_{3n+1}$ starting materials, which contain some Fe^{4+} and Ru^{4+} centers, respectively (rather than the Fe^{3+}/Ru^{5+} combination expected for a homogeneous Fe/Ru solid solution) because of poor Fe/Ru mixing. The phase separation of $Sr_{n+1}(Fe_{0.5}Ru_{0.5})_nO_{3n+1}$ phases upon reaction with CaH_2 can therefore be rationalized by observing that the introduction of ruthenium into strontium

dx.doi.org/10.1021/ic400930y | Inorg. Chem. 2013, 52, 10920–10928

iron oxide phases increases the temperature required for anion deintercalation reactions to occur (280 °C for $SrFeO_3$ compared to 400 °C for $SrFe_{0.5}Ru_{0.5}O_3$),[9,10] indicating a decline in anion mobility on ruthenium substitution. Thus, any local variation in the iron/ruthenium concentration in the $Sr_{n+1}(Fe_{0.5}Ru_{0.5})_nO_{3n+1}$ starting materials is likely to lead to a local variation in "reducibility", resulting in an inhomogeneous, multiphase reduction product.

The argument described above is built on the observation of small amounts of Fe^{4+} in the Mössbauer spectra of the reduced samples. It is possible that these small signals are artifacts of the measurement as they are weak, but given that they appear in both the $n = 1$ and $n = 2$ samples and make statistically significant contributions to the fits to the data in both cases, we think they are "real".

Transition Metal Oxidation States and Coordination Geometries. The reduction of $Sr_{n+1}(Fe_{0.5}Ru_{0.5})_nO_{3n+1}$ phases occurs via the removal of oxide ions from the $(Fe_{0.5}Ru_{0.5})O_2$ sheets present in the host materials, to yield products containing chains [or double chains in the case of $Sr_3(Fe_{0.5}Ru_{0.5})_2O_{7-x}$ phases] of apex-sharing FeO_4 planes that run along the *y*-axis of the resulting orthorhombic phases. These chains are linked by oxide ions retained within the ($^1/_2$, 0, *z*) anion sites of the $(Fe_{0.5}Ru_{0.5})O_2$ sheets [O(3) in the $Sr_2Fe_{0.5}Ru_{0.5}O_{4-x}$ phases and O(4) in the $Sr_3(Fe_{0.5}Ru_{0.5})_2O_{7-x}$ phases], and as a result, the transition metal cations reside in both planar MO_4 coordination sites and square-based pyramidal MO_5 sites as shown in Figure 8. The primary difference between the $Sr_{n+1}(Fe_{0.5}Ru_{0.5})_nO_{2.25n+1}$ and $Sr_{n+1}(Fe_{0.5}Ru_{0.5})_nO_{2.43n+1}$ phases produced upon reduction is the concentration of oxide ions within the ($^1/_2$, 0, *z*) anion sites. The $Sr_{n+1}(Fe_{0.5}Ru_{0.5})_nO_{2.25n+1}$ reduced phases have a ($^1/_2$, 0, *z*) site occupancy of 25%, resulting in a 50:50 ratio of MO_4 and MO_5 transition metal coordination sites within the materials; the $Sr_{n+1}(Fe_{0.5}Ru_{0.5})_nO_{2.43n+1}$ phases have a 43% ($^1/_2$, 0, *z*) site occupancy, yielding a 14:86 ratio of MO_4 and MO_5 sites.

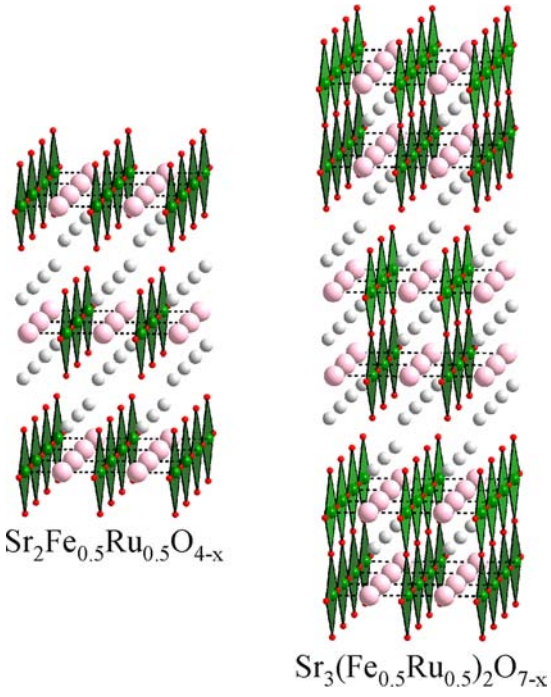

Figure 8. Structures of reduced phases $Sr_2Fe_{0.5}Ru_{0.5}O_{4-x}$ and $Sr_3(Fe_{0.5}Ru_{0.5})_2O_{7-x}$. Gray spheres represent Sr^{2+}, green squares (Fe/Ru)O_4 units, and pink spheres partially occupied ($^1/_2$, 0, *z*) anion positions.

Iron K-edge XANES data from both the $n = 1$ and $n = 2$ reduced samples indicate that all the iron centers present are in the Fe^{3+} oxidation state. When combined with the oxygen stoichiometries determined from the neutron diffraction data, this yields oxidation state combinations of $Sr_2Fe^{3+}{}_{0.5}Ru^{2+}{}_{0.5}O_{3.25}$ and $Sr_3(Fe^{3+}{}_{0.5}Ru^{2+}{}_{0.5})_2O_{5.5}$ for the $Sr_{n+1}(Fe_{0.5}Ru_{0.5})_nO_{2.25n+1}$ phases and $Sr_2Fe^{3+}{}_{0.5}Ru^{2.76+}{}_{0.5}O_{3.44}$ and $Sr_3(Fe^{3+}{}_{0.5}Ru^{2.72+}{}_{0.5})_2O_{5.86}$ for the $Sr_{n+1}(Fe_{0.5}Ru_{0.5})_nO_{2.43n+1}$ phases. Thus, these reduced iron/ruthenium phases join $SrFe_{0.5}Ru_{0.5}O_2$ as the only examples of Ru^{2+} centers in extended oxide systems.[9]

Mössbauer spectra of $Sr_2Fe_{0.5}Ru_{0.5}O_{3.35}$ and $Sr_3(Fe_{0.5}Ru_{0.5})_2O_{5.68}$ (Figures 5 and 6 and Table 4) indicate that the vast majority (~98%) of the iron centers in both samples are in the Fe^{3+} oxidation state (as indicated by the center shifts of sites 1 and 2 in Table 4) in agreement with the XANES data, with the remainder (~2%, site 3) adopting an Fe^{4+} oxidation state as discussed above. The relatively large values obtained for the quadrupole splittings of the Fe^{3+} sites (Table 4) are broadly consistent with the FeO_5 and FeO_4 coordination sites obtained from the crystallographic analysis of both $Sr_{n+1}(Fe_{0.5}Ru_{0.5})_nO_{3n+1-x}$ samples. Furthermore, the 65.3:34.6 area ratio of sites 1 and 2 extracted from the $Sr_2Fe_{0.5}Ru_{0.5}O_{3.35}$ spectrum shows a good agreement with the 66:34 ratio of FeO_5 and FeO_4 sites predicted from the crystallographic data. The area ratios obtained from the Mössbauer spectrum of $Sr_3(Fe_{0.5}Ru_{0.5})_2O_{5.68}$ match the crystallographic predictions less well (49.9:50.1 observed, 68:32 predicted). This is most likely due to the inevitable correlation in parameters that arise from fitting broad smooth spectra to multiple overlapping doublets, and with this in mind, it is possible that while the fits to the Mössbauer spectra presented appear to be robust, the parameters detailed in Table 4 may have significant errors associated with them. However, notwithstanding these caveats, the combination of crystallographic and Mössbauer data suggests that both $Sr_2Fe_{0.5}Ru_{0.5}O_{3.35}$ and $Sr_3(Fe_{0.5}Ru_{0.5})_2O_{5.68}$ contain Fe^{3+} centers in square planar coordination sites, which is highly unusual in extended oxide phases.

The Fe^{3+}/Ru^{2+} oxidation state combination observed in the $Sr_{n+1}(Fe_{0.5}Ru_{0.5})_nO_{2.25n+1}$ phases is unexpected. Typically, 4d transition metals favor higher oxidation states than 3d transition metals, as exemplified by the Fe^{3+}/Ru^{5+} oxidation state combination observed in the $Sr_{n+1}(Fe_{0.5}Ru_{0.5})_nO_{3n+1}$ starting materials,[11,21,22] and therefore, we would normally expect to observe the Fe^{2+}/Ru^{3+} oxidation state combination predicted by the standard reduction potentials of the two metals [$Fe^{3+}{}_{(aq)}/Fe^{2+}{}_{(aq)}$ = +0.77 V; $Ru^{3+}{}_{(aq)}/Ru^{2+}{}_{(aq)}$ = +0.248 V].[23] However, the Ru^{3+}/Ru^{2+} and Fe^{3+}/Fe^{2+} redox couples exhibit a strong ligand dependence, so that in the presence of ligands high in the electrochemical series, such as cyanide or 2,2′-dipyridine (bipy), the Fe^{3+}/Ru^{2+} combination is the thermodynamically favored redox combination [$Ru(CN)_6{}^{3-}/Ru(CN)_6{}^{4-}$ = +0.86 V, $Fe(CN)_6{}^{3-}/Fe(CN)_6{}^{4-}$ = +0.358 V, $Ru(bipy)_3{}^{3+}/Ru(bipy)_3{}^{2+}$ = +1.24 V, $Fe(bipy)_3{}^{3+}/Fe(bipy)_3{}^{2+}$ = +0.96 V].[24] This suggests that the transition metal coordination sites in the $Sr_{n+1}(Fe_{0.5}Ru_{0.5})_nO_x$ reduced phases help to stabilize Ru^{2+} in some way, a feature of these materials that warrants further investigation.

dx.doi.org/10.1021/ic400930y | *Inorg. Chem.* 2013, 52, 10920−10928

Magnetization data from both $Sr_2Fe_{0.5}Ru_{0.5}O_{3.35}$ and $Sr_2Fe_{0.5}Ru_{0.5}O_{3.35}$ are indicative of spin glass-like behavior at low temperatures. This glassy behavior is similar to that observed for $SrFe_{0.5}Ru_{0.5}O_2$[9] and consistent with the high levels of structural and chemical disorder in the samples that would be expected to lead to a wide range of competing magnetic couplings.

CONCLUSION

Reaction of $Sr_2Fe_{0.5}Ru_{0.5}O_4$ and $Sr_3(Fe_{0.5}Ru_{0.5})_2O_7$ with CaH_2 results in the topochemical deintercalation of oxide ions from these phases and the formation of materials with average compositions of $Sr_2Fe_{0.5}Ru_{0.5}O_{3.35}$ and $Sr_3(Fe_{0.5}Ru_{0.5})_2O_{5.68}$, respectively. Diffraction data reveal both reduced materials have undergone phase separation on reduction and consist of two-phase mixtures of topochemically reduced phases that have subtly different oxygen stoichiometries. It is proposed this phase separation is patterned by a short-range inhomogeneous distribution of iron and ruthenium in the stoichiometric starting materials.

The stoichiometries of the two $Sr_{n+1}(Fe_{0.5}Ru_{0.5})_nO_x$ materials yield average transition metal oxidation states of $M^{+2.70}$ and $M^{+2.68}$ for the $n = 1$ and $n = 2$ samples, respectively. X-ray absorption spectra reveal these values are realized as a combination of Fe^{3+} and $Ru^{2+/3+}$. Considering that the oxygen stoichiometric $Sr_{n+1}(Fe_{0.5}Ru_{0.5})_nO_{3n+1}$ phases contain Fe^{3+}/Ru^{5+} oxidation state combinations,[11,21,22] this indicates that only the ruthenium centers are reduced during the oxygen deintercalation reaction. Recent studies have shown that the soft fluorination of $Sr_3(Fe_{0.5}Ru_{0.5})_2O_7$ with CuF_2 leads to the formation of $Sr_3(Fe_{0.5}Ru_{0.5})_2O_{5.5}F_{3.5}$, which contains a combination of Fe^{3+} and $Ru^{5+/6+}$ oxidation states, as confirmed by Mössbaurer spectroscopy.[25] This demonstrates that via the application of soft reduction or oxidation chemistry, materials based on the $n = 2$ $Sr_3(Fe_{0.5}Ru_{0.5})_2O_7$ host phase can be prepared with ruthenium oxidation states ranging from Ru^{2+} to Ru^{6+} while a constant trivalent state is maintained for the iron centers.

ASSOCIATED CONTENT

Supporting Information

Plots of thermogravimetric data collected during the reoxidation of $Sr_2Fe_{0.5}Ru_{0.5}O_{3.35}$ and $Sr_3(Fe_{0.5}Ru_{0.5})_2O_{5.68}$ under flowing oxygen; observed, calculated, and difference plots from the refinement of one- and two-phase $Sr_3(Fe_{0.5}Ru_{0.5})_2O_{5.68}$ models against neutron powder diffraction data; selected bond lengths from the refined structures of $Sr_2Fe_{0.5}Ru_{0.5}O_{3.35}$ and $Sr_3(Fe_{0.5}Ru_{0.5})_2O_{5.68}$; and a comparison of two- and three-doublet fits to Mössbaurer spectra of $Sr_2Fe_{0.5}Ru_{0.5}O_{3.35}$ and $Sr_3(Fe_{0.5}Ru_{0.5})_2O_{5.68}$. This material is available free of charge via the Internet at http://pubs.acs.org.

AUTHOR INFORMATION

Corresponding Author

*Telephone: +44 1865 272623. Fax: +44 1865 272690. E-mail: michael.hayward@chem.ox.ac.uk.

Notes

The authors declare no competing financial interest.

ACKNOWLEDGMENTS

We thank E. Suard for assistance collecting the neutron diffraction data.

REFERENCES

(1) Goodenough, J. B.; Zhou, J.-S. *Chem. Mater.* **1998**, *10*, 2980.
(2) Hayward, M. A.; Green, M. A.; Rosseinsky, M. J.; Sloan, J. *J. Am. Chem. Soc.* **1999**, *121*, 8843.
(3) Adkin, J. J.; Hayward, M. A. *Inorg. Chem.* **2008**, *47*, 10959.
(4) Hayward, M. A.; Cussen, E. J.; Claridge, J. B.; Bieringer, M.; Rosseinsky, M. J.; Kiely, C. J.; Blundell, S. J.; Marshall, I. M.; Pratt, F. L. *Science* **2002**, *295*, 1882.
(5) Hayward, M. A.; Rosseinsky, M. J. *Solid State Sci.* **2003**, *5*, 839.
(6) Seddon, J.; Suard, E.; Hayward, M. A. *J. Am. Chem. Soc.* **2010**, *132*, 2802.
(7) Dixon, E.; Hayward, M. A. *Inorg. Chem.* **2010**, *49*, 9649.
(8) Dixon, E.; Hadermann, J.; Ramos, S.; Goodwin, A. L.; Hayward, M. A. *J. Am. Chem. Soc.* **2011**, *133*, 18397.
(9) Denis Romero, F.; Burr, S. J.; McGrady, J. E.; Gianolio, D.; Cibin, G.; Hayward, M. A. *J. Am. Chem. Soc.* **2013**, *135*, 1838.
(10) Tsujimoto, Y.; Tassel, C.; Hayashi, N.; Watanabe, T.; Kageyama, H.; Yoshimura, K.; Takano, M.; Ceretti, M.; Ritter, C.; Paulus, W. *Nature* **2007**, *450*, 1062.
(11) Battle, P. D.; Bollen, S. K.; Powell, A. V. *J. Solid State Chem.* **1992**, *99*, 267.
(12) O'Malley, M.; Lockett, M. A.; Hayward, M. A. *J. Solid State Chem.* **2007**, *180*, 2851.
(13) Huang, Q.; Lynn, J. W.; Erwin, R. W.; Jarupatrakorn, J.; Cava, R. J. *Phys. Rev. B* **1998**, *58*, 8515.
(14) Huang, Q.; Soubeyroux, J. L.; Chmaissem, O.; Natalisora, I.; Santoro, A.; Cava, R. J.; Krajewski, J. J.; Peck, W. F. *J. Solid State Chem.* **1994**, *112*, 355.
(15) Larson, A. C.; Von Dreele, R. B. Los Alamos National Laboratory Report LAUR 86-748; Los Alamos National Laboratory: Los Alamos, NM, 2000.
(16) Dent, A. J.; Cibin, G.; Ramos, S.; Smith, A. D.; Scott, S. M.; Varandas, L.; Pearson, M. R.; Krumpa, N. A.; Jones, C. P.; Robbins, P. E. *J. Phys.:Conf. Ser.* 2009, *190*, 012039.
(17) Ravel, B.; Newville, M. *J. Synchrotron Radiat.* **2005**, *12*, 537.
(18) Kageyama, H.; Watanabe, T.; Tsujimoto, Y.; Kitada, A.; Sumida, Y.; Kanamori, K.; Yoshimura, K.; Hayashi, N.; Muranaka, S.; Takano, M.; Ceretti, M.; Paulus, W.; Ritter, C.; Andre, G. *Angew. Chem., Int. Ed.* **2008**, *47*, 5740.
(19) Hayward, M. A.; Rosseinsky, M. J. *Chem. Mater.* **2000**, *12*, 2182.
(20) Hayward, M. A. *Chem. Mater.* **2005**, *17*, 670.
(21) Battle, P. D.; Gibb, T. C.; Jones, C. W.; Studer, F. *J. Solid State Chem.* **1989**, *78*, 281.
(22) Greatrex, R.; Greenwood, N. N.; Lal, M. *Mater. Res. Bull.* **1980**, *15*, 113.
(23) Greenwood, N. N.; Earnshaw, A. *Chemistry of the Elements*; Pergamon Press: Oxford, U.K., 1997.
(24) Vanysek, P. In *CRC Handbook of Chemistry and Physics*, 79th ed.; CRC Press: Boca Raton, FL, 1998.
(25) Denis Romero, F.; Bingham, P. A.; Forder, S. D.; Hayward, M. A. *Inorg. Chem.* **2013**, *52*, 3388.